A Load-Independent ZVS Class-E^2 Wireless Power Transfer with Receiver-side Constant-Frequency PWM Power Control

Mishima, Tomokazu

Shimizu, Shoma

Lai, Ching-Ming

(Citation)
2023 11th International Conference on Power Electronics and ECCE Asia (ICPE 2023 - ECCE Asia):1038-1043

(Issue Date)
2023-08-22

(Resource Type)
conference paper

(Version)
Accepted Manuscript

A Load-Independent ZVS Class-E^2 Wireless Power Transfer with Receiver-side Constant-Frequency PWM Power Control

1st Tomokazu Mishima
Dept. Marine Engineering
Kobe University
Kobe, Japan
mishima@maritime.kobe-u.ac.jp

2nd Shoma Shimizu
Dept. Marine Engineering
Kobe University
Kobe, Japan
211w518w@stu.kobe-u.ac.jp

3rd Ching-Ming Lai
Dept. Electrical Engineering
National Chung Hsing University
Taichung, Taiwan
pecmlai@dragon.nchu.edu.tw

***Abstract*—A compact and low-profile high frequency (HF) power converter is essential for a magnetically resonant wireless power transfer (WPT) system suitable for a small-scale electric load such as IoT equipments and medical implantable devices. This paper presents a new prototype of a class E HF inverter/active rectifier-based WPT system, where the load power control achieves only in the receiver (Rx) side while maintaining zero voltage soft-switching (ZVS) on the transmitter (Tx) side with the fixed frequency and duty cycle. The modeling-based analysis and design of PWM-controlled Rx-side class-E rectifier are originally presented in accordance with load-independent ZVS in the Transmitter (Tx)-side class-E inverter. The effectiveness of the modeling and design of the class-E^2 WPT system are verified by experiment of $1\,\mathrm{MHz}$-$8\,\mathrm{W}$ prototype, after whereby the load-independent ZVS performance of class-E inverter is demonstrated with the relevant steady-state characteristics.**

***Index Terms*—Class-E inverter / rectifier, load independence, magnetic resonance, wireless power transfer, zero voltage soft switching (ZVS).**

I. Introduction

Wireless power transfers have been drawing much attentions over the last decade due to widespread of power electronics systems in the industry, transportation, telecommunication, home and consumer appliances, and biomedical implantable devices. In particular, high frequency magnetic resonance WPT is one of the key technologies for developing the physically contactless electric power supply, e.g. the Internet-of-Things (IoT) in the next generation information technologies, pacemakers and cardiac resynchronization therapy defibrillators in the human bodies.

The technically critical issues of WPTs include how to maintain soft switching in the power devices regardless of the load conditions; load independence. For achieving the load independence, the dual LCC resonant tanks have been proposed in [1]. However, the impedances of the rectifier which operates by pulse-width-modulation (PWM) are not considered in the previous solutions, thus it is not suitable for active rectifiers in the class-E^2 WPT with the receiver (Rx)-side PWM control.

This paper presents a new analytical and modeling strategy for load-independenct soft switching class-E^2 WPT with the receiver-side. The methodology for the Transmitter (Tx)-side referred impedance of the constant frequency PWM class-E rectifier is originally proposed in this paper. Then, the design guideline of the class-E inverter can be established for higher efficiency in the class-E^2 WPT system.

The rest of this paper is organized as follows: the circuit topology and operation principle of the WPT system are described together with power control scheme in section II. Derivation of the Tx-side referred impedance of the class-E rectifier is presented in section III, then design guideline of the circuit parameters in the resonant tanks are revealed. The practical effectiveness of the analysis and design are investigated by experiment of a $1\,\mathrm{MHz}$-$10\,\mathrm{W}$ prototype in section IV, where the load-independent ZVS and steady-state characteristics of receiver (Rx)-side PWM is also verified. The power loss breakdown is also clarified and reduction of the switching power losses is actually demonstrated in detail.

II. Class-E^2 WPT System with PWM Recitifier

The circuit diagram of the proposed class-E^2 WPT system is shown in Fig.1. The Tx and Rx sides are configured by class-E HF inverter and class-E HF rectifier, respectively. The compensation resonant tank of Tx and Rx sides are comprised by the series-series resonant (SS). Note here the SS compensation is effective for the constant output voltage in the current-fed class-E HF inverter. The series capacitor C_1 is determined by referring to the phase angle of the load impedance in the class-E inverter. The series capacitor C_2 should be determined to make up the series resonance with the self inductance L_2 and the equivalent capacitance of the active rectifier and dc load at the series resonant frequency f_r, which is identical with the switching frequency f_s of the class-E inverter. The shunt capacitors C_{Q_1},C_{Q_2} assist class-E switching and ZVS in the active switches Q_1 and Q_2 with the designed parameters.

The relevant operating waveforms are depicted in Fig.2, where d_1 and d_2 are ON-time ratios of S_1 and S_2, respectively. The mode transitions and equivalent circuits are drawn in Fig. 3. The symbol ϕ_1 and ϕ_2 denote the initial phase of i_1

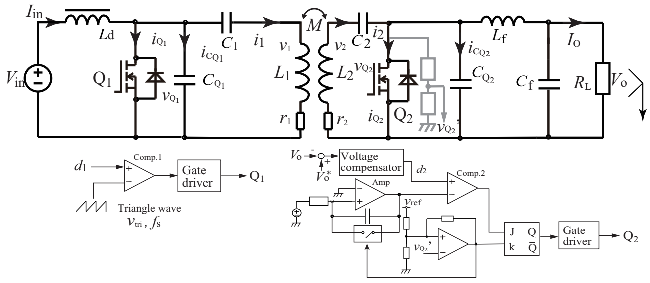

Fig. 1. Circuit diagram of the proposed class-E^2 WPT system.

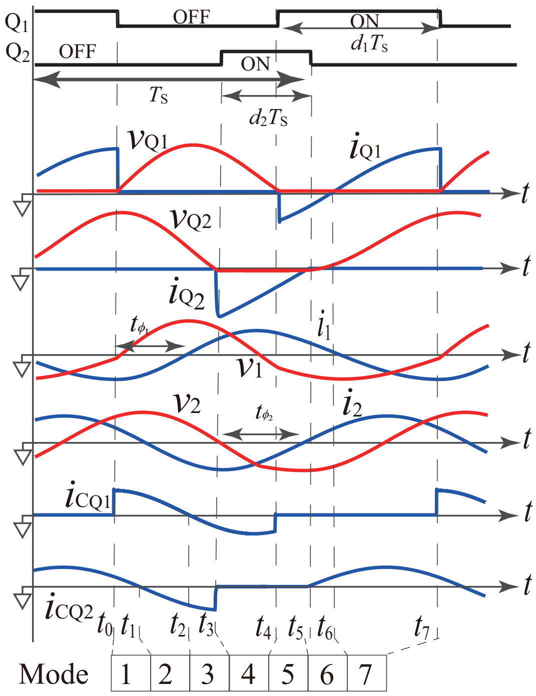

Fig. 2. Key and relevant waveforms during the switching one cycle.

and i_2 with respect to the S_1 turn-off instants and S_2 turn-on timing, respectively. The switching one cycle can be divided into the seven modes as depicted: Mode 1 ($t_0 \leq t < t_1$), *Tx magnetic energy returned and fed*, Mode 2 ($t_1 \leq t < t_2$),*magnetic energy returned*, Mode 3 ($t_2 \leq t < t_3$),*magnetic energy stored*, Mode 4 ($t_3 \leq t < t_4$),*Rx-coil current circulates*, Mode 5 ($t_4 \leq t < t_5$),*Tx and Rx coil current circulation*, Mode 6 ($t_5 \leq t < t_6$) Tx coil current circulation / Rx coils current fed-to-load, Mode 7 ($t_6 \leq t < t_7$) Tx coil current circulating in S_1 ON / Rx coils current fed-to-load

III. Analysis and Design

A. Modeling and Equivalent Circuits

The class-E active rectifier and dc load can be modeled with R_i and C_i by considering the ZVS condition $v_{Q2}(2\pi) = 0$ and the dc output voltage V_o is equal to the average value of v_{Q2} [2]. By yielding $i_2 = I_2 \sin(\omega t + \phi_s)$, the ac voltage v_{Q2} is defined as

$$v_{Q2}(\omega t) = R_i I_2 \sin(\omega t + \phi_2) + \frac{I_2}{\omega C_i}\cos(\omega t + \phi_2) \quad (1)$$

$$\frac{I_2}{\omega C_i} = \frac{1}{\pi}\int_{2\pi d_2}^{2\pi} v_{Q2}\cos(\omega t + \phi_2) d(\omega t) \quad (2)$$

where the second term of the right-hand formula is based on the fundamental frequency component in the Fourier Expansion of v_{Q2}. The voltage v_{Q2} can also be expressed by the form of integral of the displacement current as

$$\begin{aligned} v_{Q_2} &= \frac{1}{\omega C_{Q_2}}\int_{2\pi d_2}^{\omega t} i_{C_{Q_2}}\, d\tau \\ &= \frac{1}{\omega C_{Q_2}}\{I_2\left(\cos\left(2\pi d_2+\phi_2\right)-\cos\left(\omega t+\phi_2\right)\right) \\ &\quad -I_o\left(\omega t-2\pi d_2\right)\} \end{aligned} \quad (3)$$

The ratio between the Rx coil current I_2 and dc load current I_o are derived from the ZVS condition and (3) as

$$\frac{I_2}{I_o} = \frac{2\pi\left(1-d_2\right)}{\cos\phi_2 - \cos\left(\phi_2 - 2\pi d_2\right)}. \quad (4)$$

By using the relevant equations (1)-(3), the capacitance C_i can be expressed as (6). As a result, by referring to the relevant equations (1)-(4), the phase angle ϕ_2 is expressed as (5).

By neglecting the power loss in the class-E active rectifier, the power balance can be expressed as

$$R_{\mathrm{L}} {I_o}^2 = R_i\left(\frac{I_2}{\sqrt{2}}\right)^2. \quad (7)$$

Accordingly, the resistance R_i can be determined by

$$R_i = \frac{R_{\mathrm{L}}\left(\cos\phi_2 - \cos\left(\phi_2 - 2\pi d_2\right)\right)^2}{2\pi^2(1-d_2)^2} \quad (8)$$

The equivalent resistance and inductance R_{eq}, L_{eq} in Fig. 4 are obtained as

$$R_{\mathrm{eq}} = \frac{\omega_s^2\, {L_2}^2\, k^2\,\left(R_i + r_2\right)}{\left(R_i + r_2\right)^2 + \left(\omega_s\, L_2 - \frac{1}{\omega_s\, C_r}\right)^2} \quad (9)$$

$$L_{\mathrm{eq}} = \frac{k^2\, L_1\left\{\left(R_i + r_2\right)^2 - \frac{L_2}{C_r} + \frac{1}{\omega_s^2\, {C_r}^2}\right\}}{\left(R_i + r_2\right)^2 + \left(\omega_s L_2 - \frac{1}{\omega_s\, C_r}\right)^2} + \left(1 - k^2\right) L_1 \quad (10)$$

$$C_r = \frac{C_2 C_i}{C_2 + C_i} \quad (11)$$

where k denotes the coupling coefficient of Tx and Rx coils [3]. Thus, the impedance $\angle\dot{Z}_{eq}$ can be expressed by (12).

The characteristics of phase angle $\angle\dot{Z}_{eq}$ are characterized in Fig. 5 with a set of numerical examples by yielding the load ratio $\lambda = R_{L,nominal}/R_L$ [4] . The operating conditions at the lowest $\angle\dot{Z}_{eq}$ lead to the design guideline for achieving the load independent ZVS, and it should be identical with the minimum value as

$$\xi = \frac{\pi(\pi^2 - 4)}{16} = 49^\circ. \quad (13)$$

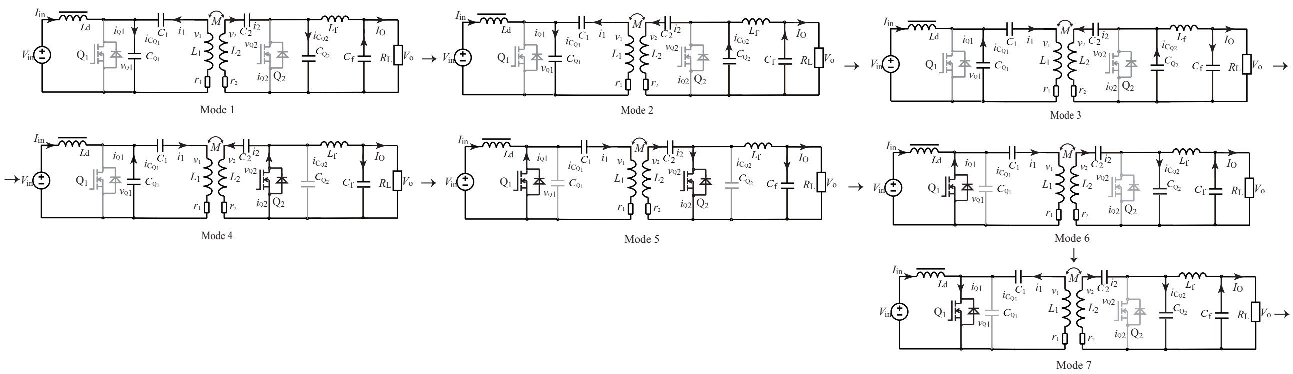

Fig. 3. Mode transition and equivalent circuits.

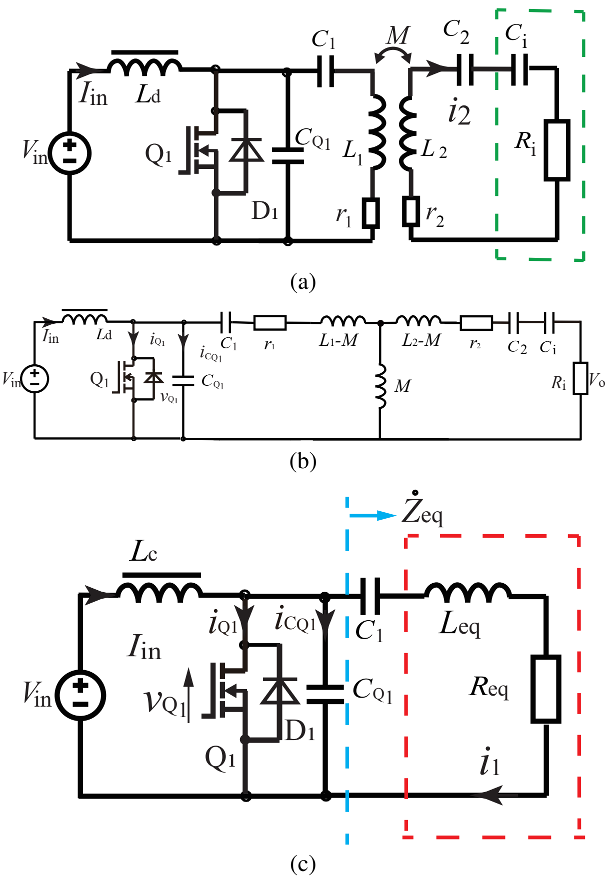

Fig. 4. Simplified equivalent circuits: (a) class-E rectifier and dc load, (b) T-shape transformation with M, and (c) Tx-side referred.

The shunt capacitor C_{Q1} of the class-E inverter can be determined from the condition of class-E (ZVS and ZVDS) as [2]

$$C_{\mathrm{Q1}} = \frac{\cos(\phi_1 + \pi d_1)}{\pi^2 R_{\mathrm{eq}} \omega (1 - d_1)} \sin(\phi_1 + \pi d_1) \cdot \sin(\pi d_1) \{\sin(\pi d_1) + \pi \cos(\pi d_1)(1 - d_1)\}. \quad (14)$$

Variations of the initial phase angle ϕ_1 for $\angle \dot{Z}_{eq}$ and d_1 are plotted by three-dimensional graphics in Fig. 6. The phase ϕ_1 increases in accordance with the increase of $\angle \dot{Z}_{eq}$ and d_1; the inductive load condition can maintain at any loads once the parameters of the reactive components are determined at the minimum load.

The design process of circuit parameters is presented in Fig. 7. By giving the power rating and relevant parameters, the phase angle, ϕ_1 is determined by referring to Fig. 6.

B. Efficiency Maximization

By using the current ratio as

$$\frac{I_{\mathrm{in}}}{I_1} = \frac{\cos(2\pi d_1 + \phi_1) - \cos\phi_1}{2\pi(1 - d_1)} \quad (15)$$

the conduction power losses in the active switch Q_1 is expressed by

$$\begin{aligned} P_{\mathrm{Q1}} &= \frac{r_{\mathrm{Q1}}}{2\pi}\int_0^{2\pi} i_{\mathrm{Q1}}^2 d(\omega t) = \frac{r_{\mathrm{Q1}}}{2\pi}\int_0^{2\pi d_1} (I_{\mathrm{in}} - I_1)^2 d(\omega t) \\ &= \frac{r_{\mathrm{Q1}} I_o^2}{2\pi} \cdot \\ &\left\{ 2\pi I_{\mathrm{in}}^2 (2 - d_2) + \frac{I_1^2}{4}[4\pi d_1 + \sin 2\phi_1 - \sin(4\pi d_1 + 2\phi_1)] \right\} \end{aligned} \quad (16)$$

The power losses in the Tx and Rx coils are defined as

$$\begin{aligned} P_{L1} &= \frac{r_1 I_1^2}{2} \\ &= \frac{r_1 I_o^2}{2k^2\omega^2 L_1 L_2 \sin^2\phi_2}\left\{ (r_2 + R_i)^2 + \left(\omega l_2 - \frac{1}{\omega C_r}\right)^2 \right\} \\ &= \frac{r_1 R_L I_o^2 (R_i + r_2)}{R_{\mathrm{eq}} R_{\mathrm{i}}} \end{aligned} \quad (17)$$

$$P_{L2} = \frac{r_2 I_2^2}{2} = \frac{r_2 I_o^2}{2\sin\phi_2^2} = \frac{r_2 I_o^2 R_{\mathrm{L}}}{R_{\mathrm{i}}} \quad (18)$$

Accordingly, the theoretical efficiency of dc-dc power conversion is expressed by

$$\tan\phi_2 = \frac{\{1-\cos(2\pi d_2)\}\left(\pi d_2^2 - 2\pi d_2 + \pi + \omega R_{\rm L} C_{\rm Q2}\right) + \{2\pi(1-d_2) + \sin(2\pi d_2)\}(1-d_2)}{\cos(2\pi d_2) + \sin(2\pi d_2)\left(\pi d_2^2 - 2\pi d_2 + \pi + \omega R_{\rm L} C_{\rm Q2}\right) - (1-d_2)} \tag{5}$$

$$\begin{aligned} C_i^{-1} = & \frac{\frac{I_{\rm o}}{I_2}\{2\pi(1-d_2)\sin(\phi_2 - 2\pi d_2) + \cos(\phi_2 - 2\pi d_2) - \cos\phi_2\} + \pi(1-d_2)}{\pi C_{\rm Q2}} \\ & + \frac{\left\{\frac{1}{2}\cos(\phi_2 - 2\pi d_2) - \cos\phi_2\right\}\sin(\phi_2 - 2\pi d_2) + \frac{1}{4}\sin(2\phi_2)}{\pi C_{\rm Q2}} \end{aligned} \tag{6}$$

$$\angle\dot{Z}_{\rm eq} = \frac{2\pi^2(1-d_1)^2 - 1 + 2\cos\phi_1\cos(2\pi d_1 + \phi) - \cos(2\pi d_1 + 2\phi_1)\{\cos 2\pi d_1 - \pi(1-d_1)\sin(2\pi d_1)\}}{4\sin\pi d_1\cos(\pi d_1 + \phi_1)\sin(\pi d_1 + \phi_1)\{(1-d_1)\pi\cos\pi d_1 + \sin\pi d_1\}} \tag{12}$$

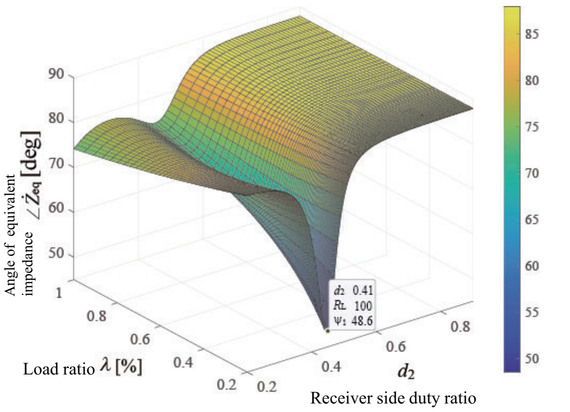

Fig. 5. Phase angle of equivalent impedance ($R_{\rm L,nominal} = 20\,\Omega$, $C_2 = 13\,$nF, $C_{\rm Q_2} = 20\,$nF, $L_1 = 2.77\,\mu$H, $L_2 = 2.87\,\mu$H).

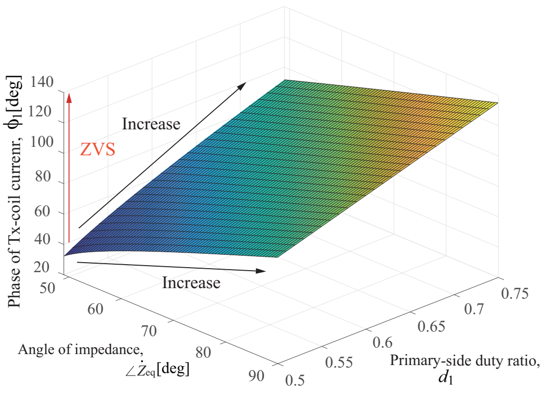

Fig. 6. Characteristics of initial phase angle $\phi_1(\angle\dot{Z}_{\rm eq}, d_1)$.

By assuming the on resistances of Q_1 and Q_2 so small and negligible as $\frac{r_{\rm Q1}}{R_{\rm L}} \approx 0$ and $\frac{r_{\rm Q2}}{R_{\rm L}} \approx 0$, (19) is reformed as

$$\begin{aligned} \eta_1 &= \frac{1}{1 + \frac{r_1(R_i + r_2)}{R_{\rm eq}R_{\rm i}} + \frac{r_2}{R_{\rm i}}} \\ &= \frac{k^2\omega^2 L_1 L_2 R_{\rm i}}{1 + r_1(R_i + r_2)^2 + k^2\omega^2 L_1 L_2 (R_i + r_2)}. \end{aligned} \tag{20}$$

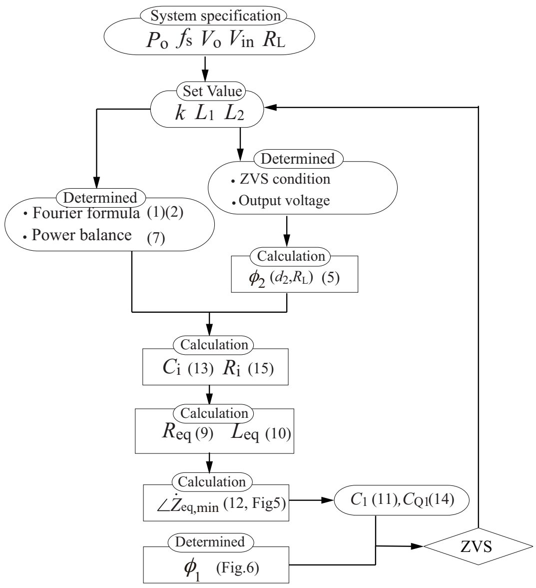

Fig. 7. Flow chart of circuit parameter design.

Thus, one can get the maximum efficiency under the condition $d\eta_1/R_l = 0$, and the equivalent resistance is expressed as

$$R_i = \sqrt{\frac{r_1 r_2^2 + k^2\omega^2 L_1 L_2 r_2}{r_1}}. \tag{21}$$

The relationship between the phase angle of Rx coil and its ON-duty cycle d_2 can be expressed as

$$\tan\phi_{2,pmax} = \frac{1 - \cos 2\pi d_2}{2\pi(1-d_2) + \sin(2\pi d_2)}. \tag{22}$$

In consequence, the shunt capacitor $C_{\rm Q2}$ can be determined

$$C_{\rm Q2} = \frac{1}{2\pi\omega R_L} \cdot \left\{1 - 2\pi^2(1-d_2^2) - \cos 2\pi d_2 + \frac{[2\pi(1-d_2) + \sin 2\pi d_2]^2}{1 - \cos 2\pi d_2}\right\}. \tag{23}$$

$$
\begin{aligned}
\eta_1 =& \frac{P_o}{P_o + P_{\mathrm{Q1}} + P_{\mathrm{Q2}} + P_{L1} + P_{L2}} \\
=& 1 \Big/ \left\langle 1 + \frac{r_{\mathrm{Q1}}}{2\pi R_{\mathrm{L}}} \left\{ 2\pi \frac{I_{\mathrm{in}}^2}{I_o^2}(2-d_2) + \frac{I_1^2}{4I_o^2}[4\pi d_1 + \sin 2\phi_1 - \sin(4\pi d_1 + 2\phi_1)] \right\} \right. \\
& \left. + \frac{r_{\mathrm{Q2}}}{2\pi R_L} \left\{ 2\pi(2-d_2) + \frac{1}{4}[4\pi d_2 - \sin 2\phi_2 - \sin(4\pi d_2 - 2\phi_2)] \right\} + \frac{r_1(R_i + r_2)}{R_{\mathrm{eq}} R_{\mathrm{i}}} + \frac{r_2}{R_{\mathrm{i}}} \right\rangle
\end{aligned} \tag{19}
$$

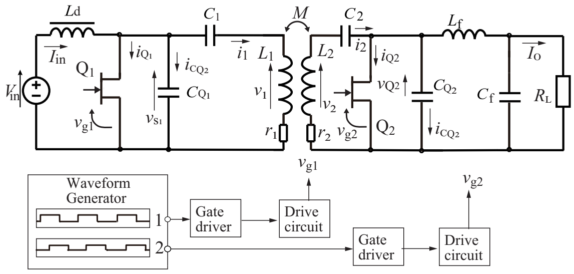

Fig. 8. System configuration of Class-E^2 WPT prototype.

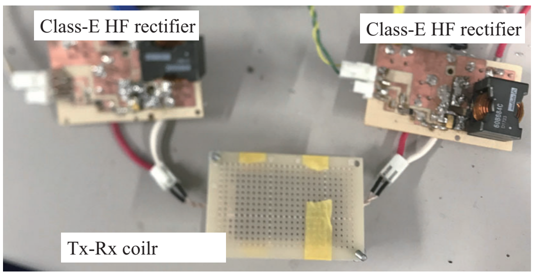

Fig. 9. Exterior appearance.

IV. Experimental Results and Evaluations

The practical effectiveness of the proposed analysis and design methodology is investigated by experiment.

The system configuration and the photograph of the prototype are portrayed in Figs. 8 and 9. The specifications of the prototype and Tx / Rx coils are indicated in TABLE I and II, respectively. The active switches in Q_1 and Q_2 are implemented with enhancement GaN-HEMT (GS66508T, 600 V, $30A@25\mathrm{C}°$, $63\,\mathrm{m}\Omega$).

The observed waveforms for the several load ratios are displayed in Figs. 10 and 11 for the rated and light load conditions. The load independent ZVS can be observed in the active switch Q_1: ZVS or ZVDS turn-on and ZVS turn-off transitions). In addition, ZCS turn-on achieves with the pseudo diode conduction mode, while ZCS (at $\lambda = 100\,\%$) or ZVS turn off attains in the active switch Q_2. Thus, the load-independent ZVS can be ensured in the prototype over the wide range of load power.

The steady-state characteristics of V_o–d_2 are drawn in Fig. 12. The load voltage V_o gradually rises in accordance with the increase of d_2 increases from 0.2 to 0.5. However, it gradually goes down in the duty cycle area over 0.5. This is due to the increase of circulating current in the secondary side rectifier, which justifies d_2 varies from 0.2 to 0.5. The actual efficiency of dc-dc power conversion is revealed in Fig. 13 together with the theoretically calculated by

$$
\eta = \frac{k^2 \omega_s^2 L_1 L_2 R_i}{1 + r_1(R_i + r_2)^2 + k^2 {\omega_s}^2 L_1 L_2 (R_i + r_2)} = 66.3\,\%. \tag{24}
$$

TABLE I
Circuit Parameters and Conditions of Prototype

Item	Symbol	Value [unit]
DC input voltage	V_{in}	12 V
DC output voltage	V_o	12 V
Rated power	P_o	8 W
Switching frequency range	f_s	1 MHz
DC inductor	L_d	$640\,\mu$H
Shunt capacitors	C_{Q1} /C_{Q2}	4.5 nF/ 17.5 nF
Series resonant capacitors	C_1/C_2	15 nF/ 10.3 nF
Output smoothing inductor	L_f	$640\,\mu$H
Output smoothing capacitor	C_f	$3\,\mu$F
Electric load resistor	$R_{\mathrm{L,nominal}}$	$20\,\Omega$

TABLE II
Tx and Rx Coils

Item	Symbol	Value [unit]
Windings turns	N_1/N_2	8 / 8
Self inductance of Tx coil	L_1	$3.35\,\mu$H
Self inductance of Rx coil	L_2	$3.32\,\mu$H
Resistance of Tx/Rx coil	r_1 /r_2	$0.24\,\mu$H/$0.35\,\mu$H
Coupling coefficient of Tx-Rx coils	k	0.1

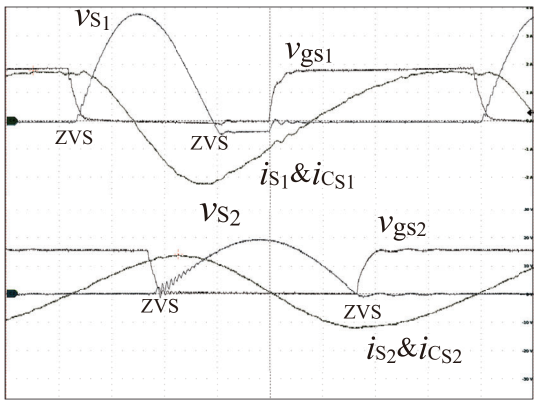

Fig. 10. Observed waveforms at the load ratio $\lambda = 100\,\%$ and $d_2 = 0.48$ (v_{Q1}, v_{Q2}: 10V/div, v_{gs1}:5V/div, i_{Q1} & i_{CQ1}:2A/div, 200 ns/div).

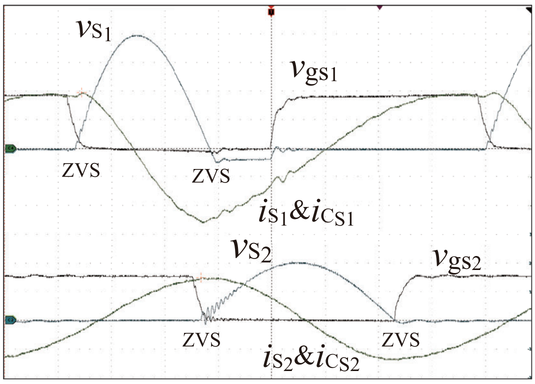

Fig. 11. Observed waveforms at the load ratio $\lambda = 25\,\%$ and $d_2 = 0.51$ (v_{Q1}, v_{Q2}: 10V/div, v_{gs1}:5V/div, i_{Q1} & i_{CQ1}:2A/div, 200 ns/div).

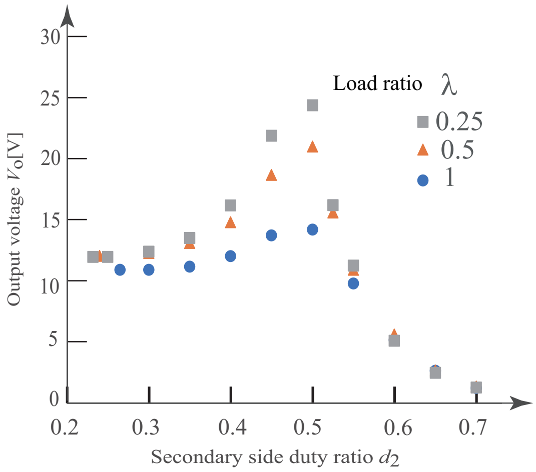

Fig. 12. Measured curves of load voltages with secondary-side PWM.

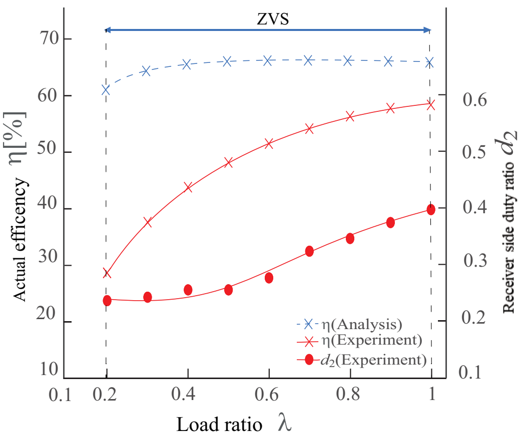

Fig. 13. Actual efficiency under the condition of constant output voltage (V_o=12V)

The maximum power efficiency is 60 % at $\lambda = 100\,\%$, which well agrees with the calculated as 66.3 % from (24). The efficiency of the class-E HF inverter is recorded as 79.2 % due to the effects of load independent ZVS regardless of the loosely coupled WPT system.

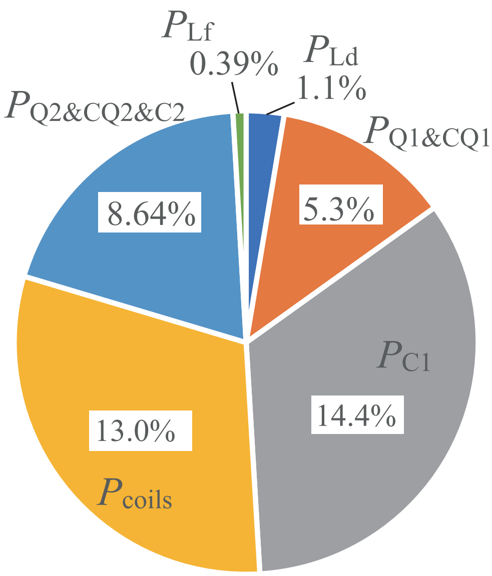

Fig. 14. Power loss breakdown.

The power loss breakdown is shown in Fig. 14. It can be known from the breakdown that the switching power losses are minimized in Q_1 and Q_2 due to the effect of load independent ZVS. The system efficiency is expected to improve by reducing the power losses in the series capacitor C_1 in the Tx side.

V. Conclusions

The load-independent ZVS class-E^2 WPT is presented in this paper featuring an active rectifier, and the parameter design scheme is proposed. The model-based equivalent circuits and the relevant equations are newly introduced, then the phase angles of the class-E inverter and rectifier are theoretically revealed, which are essential for analysis and design of the load independent ZVS in the active switches. Feasibility of the Rx-side PWM and load independent ZVS WPT system are investigated by a 1 MHz-8 W prototype, and soft switching performances, load voltage regulation and power loss analysis are revealed in details.

References

[1] J. Lu, G. Zhu, D. Lin, Y. Zhang, J. Jiang and C. C. Mi, "Unified load-independent ZPA analysis and design in CC and CV modes of higher order resonant circuits for WPT systems," *IEEE Trans. Transport. Electrif.*, vol. 5, no. 4, pp. 977-987, Dec. 2019.

[2] T. Nagashima, X. Wei, E. Bou, E. Alarcn, M. K. Kazimierczuk and H. Sekiya, " Analysis and design of loosely inductive coupled wireless power transfer system based on class-E2 dc-dc converter for efficiency enhancement, " *IEEE Trans. Circuits Sys I: Regular Papers*, vol.62, no.11, pp.2781-2791, Nov. 2015.

[3] G. Kkelis, D.C.Yates, and P. D.Mitcheson, "Class-E half-wave zero dv/dt rectifiers for inductive power transfer," *IEEE Trans. Power Electron.*, vol.32, no.11, pp.8322–8337, Nov. 2017.

[4] M. K. Kazimierczuk and D. Czarkowski, "Resonant power converters, 2nd ed. New York: Wiley, 2011.